Identification of Metal Binding Residues for the Binuclear Zinc Phosphodiesterase Reveals Identical Coordination as Glyoxalase II

Andreas Vogel, Oliver Schilling, and Wolfram Meyer-Klaucke*

EMBL Outstation Hamburg, Notkestrasse 85, 22603 Hamburg, Germany

Received February 10, 2004; Revised Manuscript Received May 5, 2004

ABSTRACT: Zinc phosphodiesterase (ZiPD) is a member of the metallo-β-lactamase family with a binuclear zinc binding site. As an experimental attempt to identify the metal ligands of *Escherichia coli* ZiPD and to investigate their function in catalysis, we mutationally exchanged candidate metal coordinating residues and performed kinetic and X-ray absorption spectroscopic analysis of the mutant proteins. All mutants (H66E, H69A, H141A, D212A, D212C, H231A, H248A, and H270A) show significantly lower catalytic rates toward the substrate bis(*p*-nitrophenyl)phosphate. Substrate binding, represented by the kinetic value K', remains unchanged for six mutants, whereas it is increased 3−4-fold for H231A and H270A. Accordingly, these two residues are supposed to be involved in substrate binding, whereas the others are more important for catalytic turnover and thus are assumed to be involved in zinc ligation. Structural insight into the metal binding of D212 was gained by zinc K-edge extended X-ray absorption fine structure (EXAFS). The sulfur coordination number of the cysteine mutant was found to be 1, demonstrating binding to both zinc metals in a bridging mode. Taken together with two residues from a strictly conserved sequence region within the metallo-β-lactamase family, the metal site of ZiPD is proposed with H64, H66, and H141 coordinating ZnA, D68, H69, and H248 coordinating ZnB, and D212 bridging both metals. Surprisingly, the same coordination sphere is found in glyoxalase II. This is further substantiated by comparable EXAFS spectra of both native enzymes. This is the first example of the same metal site in two members of the metallo-β-lactamase domain proteins catalyzing different reactions. The kinetic analysis of mutants provides unexpected insights into the reaction mechanism of ZiPD.

The protein encoded by the ElaC gene in *Escherichia coli* was recently characterized as a binuclear zinc phosphodiesterase (ZiPD)[1] (*1*). Homologous genes are found in all domains of life. In higher eukaryotes two ElaC genes exist, one with a size similar to ZiPD (ElaC1) and one that has approximately twice the size (ElaC2). ElaC2 was identified as a candidate prostate cancer susceptibility gene, and the function of the homologous gene in yeast was shown to be essential (*2*). The C-terminal part of ElaC2 shows sequence homology to ElaC1, and the N-terminal part can also be aligned to ElaC1, however with significantly lower homology. This gives rise to the suggestion that ElaC2 might have evolved from gene duplication. Since the ElaC1 homologue ZiPD consists of a dimer in solution (*1*), this oligomerization state could be conserved in ElaC2 by a covalent linkage.

ZiPD effectively hydrolyzes the artificial substrate bis(*p*-nitrophenyl)phosphate (bpNPP) (*1*). A physiological substrate has recently been identified for the ElaC genes from archaea and eukaryotes (*3*, *4*). These ElaC gene products act as tRNA 3′ processing endoribonucleases (RNase Z), cleaving the phosphodiester bond between the 3′ trailer and the mature tRNA. However, the mechanism of 3′ tRNA maturation is different in bacteria and eukaryotes. While in the latter a single endonucleolytic cut takes place, the maturation of the 3′ terminus in bacteria is a multistep process that utilizes different endo- and exonucleases and is intensively characterized in *E. coli* (*5*, *6*). A recent paper describes the RNase Z activity of the ZiPD homologous protein from the Gram-positive bacterium *Bacillus subtilis* (*7*). In contrast to *E. coli* the CCA discriminator is not present in all tRNA genes of *B. subtilis*. Since the *B. subtilis* RNase Z is inhibited by the CCA discriminator and thus functions mainly on tRNA precursors without the discriminator (*7*), it is uncertain if the *E. coli* ElaC gene product is also involved in tRNA maturation, despite their high sequence homology.

Sequence alignments place ZiPD in the structural family of metallo-β-lactamases, a rapidly growing family of binuclear metalloproteins which perform a variety of diverse functions (*8*, *9*). The majority of the members are hydrolytic enzymes which cleave the amide bonds of β-lactams and ester bonds of thioesters and nucleic acids (*10*−*12*). The metal utilized for these reactions was shown to be zinc in the case of metallo-β-lactamases, ZiPD, and glyoxalase II (GlxII) (*1*, *10*, *11*). However, GlxII is also capable of utilizing iron and manganese for catalysis (*13*). In addition to the hydrolytic enzymes, the redox enzyme rubredoxin:oxygen oxidoreductase (ROO) was identified as a member of the metallo-β-lactamase family (*14*). In this multidomain protein, the redox cofactors are a flavin mononucleotide, which is bound in a flavodoxin domain, and two iron atoms in the metallo-β-lactamases domain.

* Corresponding author. Tel: +49 40 89902124. Fax: +49 40 89902149. E-mail: wolfram@embl-hamburg.de.

[1] Abbreviations: ZiPD, zinc phosphodiesterase; GlxII, glyoxalase II; ROO, rubredoxin:oxygen oxidoreductase; bpNPP, bis(*p*-nitrophenyl)-phosphate; EXAFS, extended X-ray absorption fine structure.

10.1021/bi049703+ CCC: $27.50
Published on Web 07/22/2004

The metal binding sites vary between the yet structurally characterized members of metallo-β-lactamase domain proteins (*10*, *11*, *14*−*16*). Coordination by three histidines for metal site A is a common feature of the hydrolytic enzymes. Only in the iron binding redox enzyme ROO is one of these histidines replaced by glutamate. The coordination of metal site B shows higher diversity, with different combinations of cysteine, histidine, and aspartate residues in a 5- or 6-fold coordination. The two metals are bridged by a hydroxide and in some cases additionally by an aspartate residue. The sequence motif characteristic for metallo-β-lactamase domain proteins is HxHxDH (*9*). In this motif the first three amino acids are strictly conserved as metal binding ligands, whereas the fourth coordinates ZnB in metallo-β-lactamases L1 and GlxII only (*10*, *16*). The overall homology between the different metallo-β-lactamase domain proteins is generally less than 24%. Besides the area surrounding the strongly conserved HxHxDH motif, the sequences cannot be unequivocally aligned. This is exemplified by the different predictions of Zn binding residues for GlxII and ZiPD on the basis of multiple sequence alignments of the metallo-β-lactamase family (*8*, *9*, *17*).

To investigate the relationship between activity and the metal coordination within the metallo-β-lactamase family, we initiated an attempt to identify the zinc binding residues of ZiPD by kinetic and EXAFS spectroscopic analysis of site-directed mutants. In addition to the metal coordination, two histidines were identified which are involved in substrate binding. The resulting model of ZiPD's Zn site is identical to the metal coordination sphere in GlxII. This is further substantiated by comparison of the EXAFS spectra of these enzymes. This is the first example of an identical metal site displaying different reactions within the metallo-β-lactamase family.

EXPERIMENTAL PROCEDURES

Materials. Except when stated otherwise, all fine chemicals were purchased from Sigma. Restriction enzymes were from New England Biolabs. Oligonucleotides were synthesized by Proligo (Paris, France). DNA sequencing was performed by MWG (Ebersberg, Germany).

Sequence Alignment. Sequences homologous to ZiPD were identified by BLAST searches in public sequence databases. The primary multiple sequence alignment was generated by ClustalW (*18*) (http://www.ebi.ac.uk/clustalw). This was subsequently refined by eye in the program GeneDoc (http://www.psc.edu/biomed/genedoc), which was also used to color the alignment.

Site-Directed Mutagenesis. Site-directed mutagenesis was performed using the procedure described in the Quikchange site-directed mutagenesis protocol (Stratagene) using KOD Hot Start polymerase (Novagen). The vector pETM-ZiPD harboring the *E. coli* ElaC gene (*1*) was used as a template. In addition to the desired mutation, silent mutations were introduced in order to obtain a new restriction site to allow for easy screening of the mutant vector (Table 1). This was guided by the World Wide Web-based computer program The Primer Generator (*19*) (http://www.med.jhu.edu/medcenter/primer/primer.cgi). The complete insert was sequenced to verify that no unintentional mutations occurred.

Protein Expression and Purification. Protein expression and purification of the recombinant proteins followed an optimized protocol to that described in ref *1*. Zinc was added to the lysis buffer only at a concentration of 0.1 mM. Since we observed protein instability in the presence of this zinc concentration in the purified sample, it was omitted from the following purification steps. As reducing agent, 0.2 mM DTT was present throughout the purification. A final gel filtration chromatography was performed in 50 mM Tris-HCl, pH 7.4, 150 mM NaCl, and 10% (v/v) glycerol. The same expression and purification protocol was used for all mutants and the wild-type enzyme. This protocol consistently achieved wild-type ZiPD with a specific phosphodiesterase activity of >100 units/mg.

Table 1: Sequences of Primers Used To Generate Mutants of ZiPD[a]

mutation	sequence (5′ → 3′)	new restriction site
H69A	TCATGGCGAT**GC**TCT**C**TT**C**GGTTTACCCG	*Ear*I
H66E	TCAGTCACCT**CG**AG**G**GCGATCATCT	*Xho*I
H141A	GCTTATCCGCT**C**GA**GGC**CCCACTGGAATGT	*Xho*I
D212A	GCTATTTTCGGCG**CC**ACCGGCCCCTGCGAT	*Sfo*I
D212C	GCTATTTTCGGC**TG**TAC**G**GGCCCCTGCGAT	*Apa*I
H231A	GATGTCATGGTG**GC**CGAAGCGACGCTGGAT	none
H248A	ATAGTCGCGGC**GCG**AGCTCTACACGCCA	*Sac*I
H270A	CTAATCATTAC**TGCA**GTCAGCTCGCGCTAT	*Pst*I

[a] Modified bases are in bold type; the introduced restriction site is underlined. Only the forward primer is shown; the reverse primer corresponds to the complementary one.

Kinetic Measurements. Phosphodiesterase activity was measured using bis(*p*-nitrophenyl)phosphate (bpNPP) essentially as described in ref *1*. The reaction buffer was 50 mM Tris-HCl, pH 7.4, and 0.1% Triton-X-100. One unit of activity corresponds to 1 μmol of *p*-nitrophenol liberated per minute at 22 °C. The kinetic parameters K' and k_{cat} and the Hill coefficient, n_H, were extracted from the dependence of the initial reaction velocities on the substrate concentration, c_S, applying the Hill equation (*20*) in the form:

$$v = V_{max} \frac{{c_S}^{n_H}}{K' + {c_S}^{n_H}}$$

by nonlinear regression analysis implemented in the program Origin 5.0 (Microcal, Northampton, MA).

X-ray Absorption Spectroscopy. The X-ray absorption spectrum at the Zn K-edge for the ZiPD D212C mutant was recorded in fluorescence mode at the EMBL bending magnet beamline D2 (DESY, Hamburg, Germany) equipped with a Si(111) double crystal monochromator, a focusing mirror, and a 13 element Ge solid-state fluorescence detector (Canberra). The protein was kept in 50 mM Tris-HCl, pH 7.4, 150 mM NaCl, and 10% (v/v) glycerol and was concentrated to a final concentration of ca. 1 mM. The protein solution was filled into plastic sample holders covered with polyimid windows, frozen in liquid nitrogen, and kept at 30 K during the experiment. Harmonic rejection was achieved by a focusing mirror with a cutoff energy of 21 keV and a monochromator detuning to 70% of peak intensity. Dead time correction was applied. Saturation was not observed because the dead time was always below 20%. The energy axis of each scan was calibrated by using the Bragg reflections of a static Si(220) crystal in back-reflection geometry (*21*). Averaging of 30 scans and data reduction

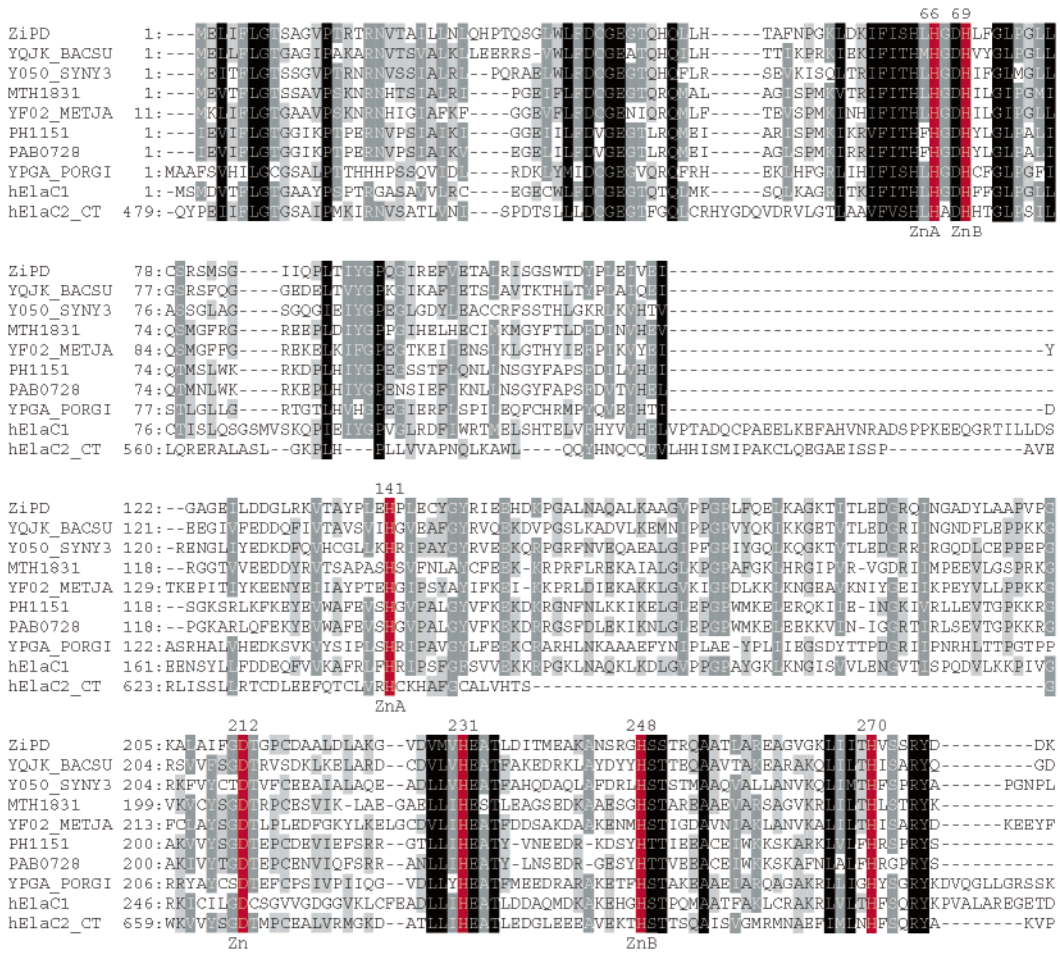

FIGURE 1: Candidate zinc binding residues from multiple sequence alignment of close ZiPD homologues. Multiple sequence alignment was calculated by ClustalW and subsequently refined by eye. The GenBank accession number of ZiPD is NP_754698, of hElaC1 NP_061166, and of hElaC2 NP_060597. The remaining sequences are defined by their Swiss-Prot entry name or gene name, respectively. The amino acid position is indicated after the name. Darker shading represents more conserved residues. The residues chosen for site-directed mutagenesis are shown in red with its position in the ZiPD sequence marked on top. Binding to zinc A (ZnA), zinc B (ZnB), or to both zinc atoms (Zn), as detected in this study, is shown below the respective position. The first 340 residues of the alignment are shown.

were performed with the EXPROG software package (C. Hermes and H. F. Nolting, EMBL-Hamburg) using $E_{0,Zn} = 9660$ eV. The EXAFS spectrum was analyzed with EXCURV98 (*22*). The *R*-factor was used as a measure for the goodness of the fit and is defined by Binsted et al. (*22*). The model for D212C was based on the previous EXAFS characterization of wild-type ZiPD, which gave proof for a binuclear zinc site consisting of an average of 4 to 5 N/O ligands (*1*). For the present model, ligand types as well as coordination numbers were varied manually, whereas the distances, the Debye−Waller factors, and the Fermi energy offset were refined. Histidine ligands are represented by an imidazole group as provided by EXCURV98. Due to the limited resolution of EXAFS at $\Delta k = 3-12$ Å^{-1} and in order not to overinterpret the spectrum, distances to first shell N and O atoms were refined collectively. To partially compensate for eventual inaccuracies of the imidazole group, it was subjected to a restrained refinement as described by Feiters et al. (*23*). Only minor alterations of the imidazole group were observed; for this reason the final model was based on constrained refinement, hence minimizing the number of free parameters.

RESULTS

Selection of Mutants. From sequence database searches, seven sequences with more than 45% homology to *E. coli* ZiPD were chosen for a multiple sequence alignment. In addition, the translated human ElaC1 and ElaC2 sequences were included in this alignment (Figure 1). The EXAFS analysis of wild-type ZiPD revealed a donor set of nitrogen and oxygen atoms only. The ZiPD metal binding site does not contain ligating sulfur atoms (*1*). Thus, we searched for conserved histidine and aspartate residues within the multiple sequence alignment as potential metal binding amino acids. Within the metallo-β-lactamase signature motif HxHxDH (amino acids 64−69 of ZiPD) the first three residues are strictly conserved for metal binding and were not chosen for site-directed mutagenesis. Residues amino terminal of the metallo-β-lactamase signature motif do not participate in metal ligation in any metallo-β-lactamase. The H66E mutation was chosen because it represents the sequence motif in ROO. Since the homologous residues for H69 do not always participate in the zinc coordination, the alanine mutant was created and analyzed. The remaining conserved residues were H141, D212, H231, H248, and H270. Replacement by

Table 2: Kinetic Constants of ZiPD Mutants toward bpNPP[a]

sample	rel k_{cat} (%)	k_{cat} (s^{-1})	K' (mM)	k_{cat}/K' (mM^{-1} s^{-1})	n_H
wild type	100.00	60 ± 6	6 ± 1	9.9	1.8 ± 0.2
H66E	0.00	0.00			
H69A	3.51	1.7 ± 0.2	8 ± 2	0.2	1.8 ± 0.2
H141A	0.14	0.06 ± 0.03	8 ± 1	0.01	1.6 ± 0.3
D212A	0.11	0.05 ± 0.02	6 ± 1	0.01	1.8 ± 0.4
D212C	0.44	0.2 ± 0.1	7 ± 2	0.03	1.5 ± 0.2
H231A	8.03	4 ± 2	21 ± 3	0.2	1.8 ± 0.2
H248A	0.11	0.05 ± 0.01	3 ± 1	0.02	1.2 ± 0.2
H270A	0.05	0.02 ± 0.01	27 ± 5	0.01	1.1 ± 0.2

[a] Substrate-dependent activity of purified ZiPD mutants was measured and analyzed according to the Hill equation as described in Experimental Procedures. Activity was measured for at least three independent preparations. n_H = Hill coefficient.

alanine was done for functional analysis. A cysteine mutant of D212 was generated for EXAFS analysis to probe an assumed bridging binding mode.

Purification of ZiPD Mutants. All mutants were expressed at a similar level as wild-type ZiPD in a soluble form from the homologous overexpression system. All mutants eluted from the final size exclusion column at a similar volume which is characteristic for a protein dimer. CD spectroscopy showed no significant changes in secondary structure induced by the mutations (see Figure 1 in Supporting Information).

Phosphodiesterase Activity of Mutants. All mutants show significant loss of phosphodiesterase activity (Table 2). The mutant H66E was apparently inactive. A relative k_{cat} of more than 1% was observed only for mutation of H69 and H231. The most active mutant was H231A with a relative k_{cat} of 8%. The K' value, indicative for substrate affinity, was significantly raised for mutation of residues H231 and H270. Replacement of H231 by alanine increases K' from 6 to 21 mM and replacement of H270 by alanine to 27 mM. This shows that H231 and H270 are located at sites that interact with the substrate. A reduction of K' that goes along with a decrease of n_H was observed for H248A.

EXAFS Spectroscopy of D212C. Residue D212 of ZiPD could occupy a homologous position as D135 in GlxII. For this residue, the crystal structure of human GlxII shows a coordination to both metal atoms (*10*). This gave rise to the assumption of D212 bridging both metals in ZiPD as well. The mutation of coordinating N/O ligands to sulfur ligands allows for their eventual identification by EXAFS spectroscopy. For this reason, the ZiPD residue D212 was mutated to cysteine, and the resulting D212C protein was characterized by EXAFS spectroscopy (Figure 2).

ZiPD was previously characterized as having a binuclear zinc site consisting of N/O ligands without a coordinating sulfur (*1*). D212C has a zinc stoichiometry comparable to wild-type ZiPD (data not shown). In comparison to wild-type ZiPD, the Zn K-edge EXAFS of D212C shows phase and amplitude differences (Figure 2). The Fourier transform demonstrates that the first shell peak of D212C is wider and more intense. It also extends by approximately 0.2 Å to higher first shell ligand distances. The outer shell peaks occur essentially at similar distances and with comparable intensities. Hence, the D212C mutation mainly affects the first shell coordination. The D212C EXAFS spectrum is best fitted with a model that includes a ligating sulfur atom with a coordination number of 1 (Table 3). A 1-fold occupancy for the only

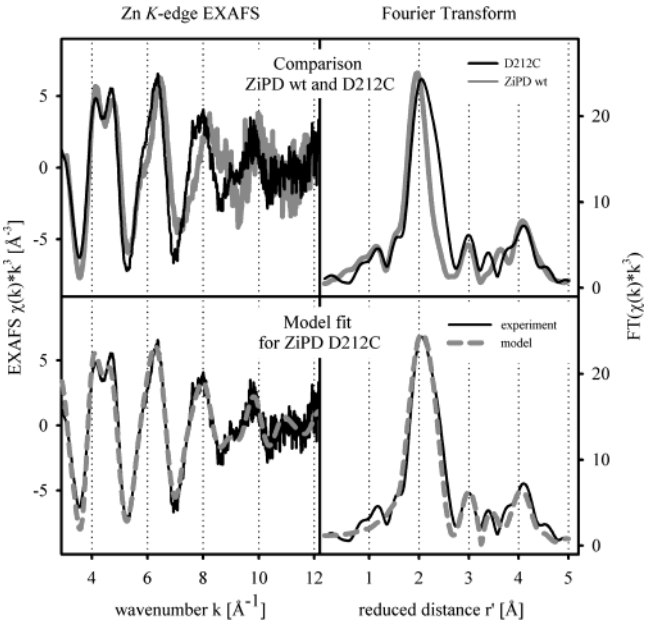

FIGURE 2: EXAFS and Fourier transform of D212C. EXAFS (left) and the corresponding Fourier transform (right) of D212C (dark line). On the top the spectrum of the mutant is compared to the wild-type ZiPD spectrum taken from ref *1* (gray line). The calculated spectrum for D212C based on the model given in Table 3 is shown in gray lines at the bottom. $\chi(k)$ is the EXAFS amplitude; r' is the metal−ligand distance corrected for first shell phase shifts; au = arbitrary units; FT = Fourier transform amplitude; ZiPD wt = ZiPD wild type.

Table 3: Average Zinc Coordination of D212C As Derived by EXAFS Data Analysis in Comparison to Previously Published EXAFS Analysis of ZiPD Wild Type[a]

		ZiPD D212C			ZiPD wild type[b]		
ligand	atom[c]	N	r[d] (Å)	σ^2 (Å^2)	N	r (Å)	σ^2 (Å^2)
His	N	2.5	2.02 (2)	0.007 (2)	2.0	1.99 (2)	0.007 (1)
	C_1		3.01	0.004 (3)		3.00	0.006 (3)
	C_1		3.08	0.004 (3)		3.06	0.006 (3)
	C_2		4.17	0.004 (3)		4.13	0.004 (1)
	N_2		4.20	0.004 (3)		4.18	0.004 (1)
Asp/Glu	O				1.0	1.99 (2)	0.007 (1)
	C_1					2.92	0.006 (3)
	O_1					3.17	0.006 (3)
	C_2					4.30	0.004 (1)
H_2O/OH^-, Asp/Glu	O	1.5	2.02 (2)	0.007 (2)	1.5	1.99 (2)	0.007 (1)
Cys	S	1.0	2.28 (2)	0.004 (2)			
Zn	Zn	1.0	3.23 (5)	0.010 (5)	1.0	3.32 (3)	0.01 (1)

[a] N is the coordination number, r is the mean interatomic distance, and σ^2 is the Debye−Waller factor. Numbers in parentheses represent the uncertainties of the last digit. The R-factor of the model for ZiPD D212C is 32.5%, and the Fermi energy offset is −8 (1) eV. The model for ZiPD wild type was previously published and has an R-factor of 31.9% and a Fermi energy offset of −6.47 eV (*1*). Quantitative EXAFS analysis determines coordination numbers with an accuracy of 20%, as has been found by a reference study on model compounds (*40*). This intrinsic error is not explicitly stated. The fitting procedure is described in Experimental Procedures. [b] Data taken from ref *1*. [c] For outer shell atoms of the imidazole group with comparable distances to the Zn center, the Debye Waller factors have been refined collectively. This is indicated by identical subscripts. [d] Distances to first shell N and O ligands as well as their Debye Waller factors were refined collectively to not overinterpret the spectrum.

sulfur atom at a binuclear zinc binding site implies that the sulfur atom bridges both zinc ions. Accordingly, it is assumed

that D212 acts as a bridging residue in the case of wild-type ZiPD.

This analysis is supported by comparison to EXAFS spectra of further proteins belonging to the metallo-β-lactamase family. In the case of the *Bacillus cereus* (strain 569/H/9) metallo-β-lactamase a ligating sulfur atom coordinates to only one of the two zinc ions in the binuclear active site (*24*). The resulting average coordination with 3.5 N/O ligands and 0.5 sulfur ligand leads to a Fourier transform first shell peak with significant differences to D212C: it is narrower and located at about 2.0 Å instead of 2.2 Å as is the case for D212C (not shown).

The first shell distances of the refined model (Table 3) are within the range of zinc coordination bond lengths found in high-resolution structures of model compounds and metalloproteins (*25*, *26*). The Debye−Waller factors of the outer shell imidazole atoms are assumed to not be elevated enough. This is attributable to the fact that within the model the imidazole group accounts for all outer shell atoms, neglecting further ligating amino acids. However, EXAFS models with an increased number of outer shell atoms did not lead to decreased *R*-factors. In summary, EXAFS analysis of D212C indicates that D212 bridges the binuclear metal binding site.

A neighboring zinc atom is indicated by the EXAFS analysis. The metal−metal contribution is of low significance but obvious in the form of an additional Fourier transform peak between 3 and 4 Å. A similar situation was reported for the Zn K-edge EXAFS of glyoxalase II, another metallo-β-lactamase domain protein with a bimetal site. Glyoxalase II also incorporated iron and manganese. Electron paramagnetic resonance spectroscopy clearly detected Fe(III)Fe(II) and Mn(II)Mn(II) centers while the metal−metal contribution in the EXAFS analysis was also of low significance. In summary, the Zn K-edge EXAFS of ZiPD D212C is indicative for a bizinc site. Metal−metal contributions in X-ray absorption spectroscopy may be hidden due to phase cancellation by backscattering from light elements, e.g., belonging to ligating imidazole groups (*27*, *28*). In the case of ZiPD D212C, plotting the single contributions to the theoretical EXAFS spectrum reveals that the zinc−zinc contribution is most prominent in the region of $k = 6-10$ Å^{-1}. In the same region multiple backscattering from the imidazole groups leads to an extraordinarily irregular EXAFS pattern (Figure 3).

In comparison to the EXAFS analysis of wild-type ZiPD, D212C has a significantly shorter Zn−Zn distance which corresponds nicely to extended distances of first shell N/O ligands to the zinc center. It appears that the replacement of a bridging aspartate by a cysteine contracts the Zn−Zn distance. The Zn−N/O distances are still in the typical range (*25*, *26*).

In good agreement with the determined alterations of the coordination sphere, the X-ray absorption near-edge structure (XANES) spectra of ZiPD D212C and wild type show significant differences (Figure 4). In both cases, two peaks are present at approximately 9667 and 9672 eV, respectively. Several reports concerning Zn K-edge XANES for proteins with mixed N/O/S zinc coordination spheres have established a trend on how the number of ligating sulfur atoms influences the Zn K-edge XANES (*29*−*32*). As a trend, an increase in the number of ligating sulfur atoms leads to a more intense

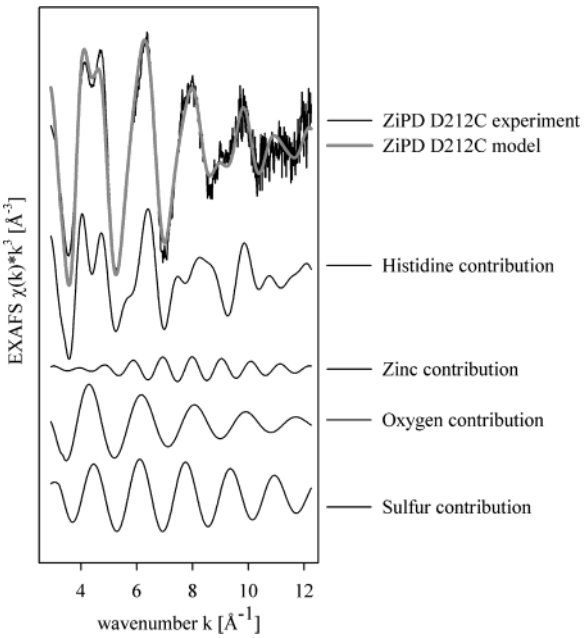

FIGURE 3: Single contributions to the theoretical EXAFS spectrum of ZiPD D212C. Single contributions to the theoretical EXAFS spectrum of ZiPD D212C are as stated in Table 3. All spectra are equally scaled.

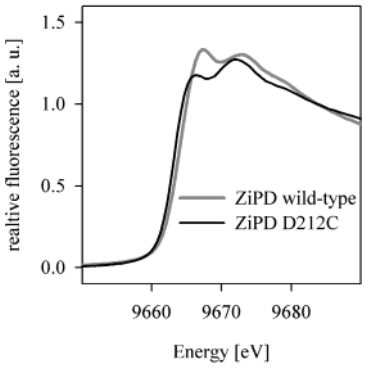

FIGURE 4: Influence of the sulfur coordination on the zinc absorption edges of ZiPD. Normalized Kα fluorescence of ZiPD D212C (black line) and wild type (gray line). Data for ZiPD wild type are taken from ref *1*.

first XANES peak (here approximately 9667 eV) and a less intense second XANES peak (here approximately 9672 eV). This is not the case for ZiPD: D212C, in comparison to ZIPD wild type, has a less intense first XANES peak and a similar intense second XANES peak. The white line of D212C also rises at a slightly lower energy than for ZiPD wild type. Both observations underline the sensitivity of XANES spectra to the metal coordination geometry (*33*). In the case of ZiPD D212C, the contracted Zn−Zn distance is indicative for geometrical alterations. XANES spectra as such provide only limited information about the type of first shell metal ligands due to the strong dependence on the local geometry. Model compounds with either 4 nitrogen or 4 sulfur ligands can have extraordinarily similar XANES spectra [tetrakis(2-methylimidazole)zinc(II) perchlorate and zinc(II) ethylxanthate] while the XANES spectra of model compounds with a similar set of ligands (N_2S_2) can exhibit vast differences [2,3-bis((mercaptophenyl)amino)butane zinc(II) and (2,3-bis((mercaptophenyl)amino)butadiimine zinc(II)] (*30*).

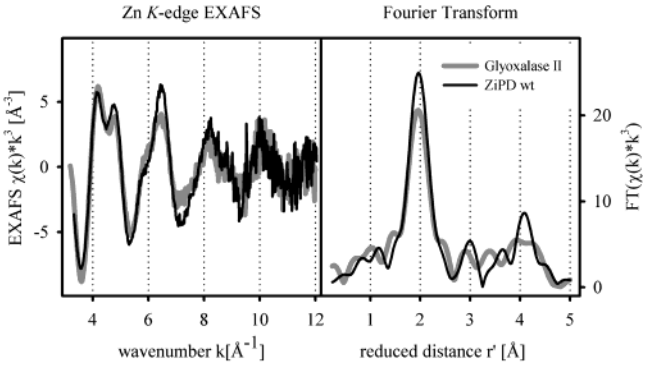

FIGURE 5: Comparison of the EXAFS spectra of ZiPD and glyoxalase II. Raw EXAFS data (left) and the corresponding Fourier transform (right) for zinc forms of wild-type ZiPD (black line) and GlxII (gray line) are taken from the refs *1* and *13*. ZiPD wt = ZiPD wild type.

Comparison of the EXAFS Spectra of ZiPD and GlxII. The kinetic and EXAFS spectroscopic analysis of the ZiPD mutants gave rise to the assumption that the coordination sphere is similar to that of GlxII. The EXAFS spectra of both enzymes are in complete agreement with that proposal. The Zn K-edge EXAFS spectra of ZiPD and glyoxalase II are essentially in phase and have mostly amplitude differences (Figure 5). Accordingly, the Fourier transform demonstrates comparable first shell distances for both enzymes. The first shell peak is less intense for glyoxalase II, this is most likely arising from different sample states. While ZiPD was measured as solution, glyoxalase II was lyophilized, eventually resulting in a loss of a coordinated water molecule. Both spectra share main features such as the double peak between 4 and 5 $Å^{-1}$ attributed to the multiple scattering within the imidazole ring. Minor phase related divergences are apparent at 5, 6, and 7 $Å^{-1}$. The comparison of the ZiPD and GlxII Zn K-edge EXAFS spectra is indicative of structurally similar, yet not identical metal binding sites. This complements the identification of D212 as a bridging residue in the ZiPD bizinc site, reminiscent of the bridging D135 in human GlxII.

DISCUSSION

Within the metallo-β-lactamase family, most mechanistic studies were performed for β-lactam hydrolyzing enzymes. The current model of the reaction mechanism of β-lactam cleavage by metallo-β-lactamase involves activation of a bridging hydroxide as the nucleophile by the zinc atoms in addition to activation and preorientation of the substrate by the binuclear site (*34*). Thus, the structural integrity and the electronic properties of the binuclear site are the keys for catalysis. Any change in the zinc ligands would therefore drastically affect the catalytic properties. The role of the only zinc atom in mononuclear metallo-β-lactamases is activation of the nucleophilic hydroxide and polarization of the carbonyl bond of the substrate (*34*). A change in mechanism was observed for the binuclear metallo-β-lactamases where it was shown by Wang et al. (*35*) for nitrocefin cleavage that an unusual anionic intermediate is stabilized by ZnB following nucleophilic attack. Thus, in a simplified general model, ZnA activates mainly the nucleophile, whereas ZnB interacts mainly with the substrate. The fact that the 3-His coordination is conserved in all hydrolytic metallo-β-lactamase domain proteins and the ZnB site is much more variable supports this view. The only ZiPD mutant with apparently no phosphodiesterase activity was H66E, a ZnA ligand which is part of the metallo-β-lactamase consensus sequence. This supports the view that the 3-His coordination is invariant for a hydrolytic purpose. Since H66E mimics the situation in ROO, an iron-utilizing redox enzyme of the metallo-β-lactamase family, this exchange might be the prerequisite for this domain binding iron and being able to act as a redox enzyme.

H66 was readily identified as the metal ligand in ZiPD by sequence comparison. In the consensus pattern $H_{64}XH_{66}$-$XD_{68}H_{69}$ (numbering for ZiPD) the first three residues are all metal binding ligands. The last histidine binds a metal (always ZnB) in two members only. The low activity of H69A clearly shows an involvement in phosphodiester cleavage by ZiPD. The same is true for H141. Its distance to the consensus pattern is similar to the third His of ZnA in other metallo-β-lactamase domain proteins (*8*). Thus, we propose that H141 forms together with H64 and H66 the 3-His site in ZiPD. A metal binding aspartate in metallo-β-lactamase domain proteins can bridge both metals, as in GlxII, or bind only to ZnB, as in the metallo-β-lactamase of *Stenotrophomonas maltophila* (formerly *Xanthomonas maltophila*). To test the binding mode of D212 in ZiPD, we analyzed the EXAFS of the D212C mutant. The coordination number for sulfur yields 1, which is in agreement with a bridging binding mode. This shows that the backbone of residue 212 is correctly positioned for a bridged binding. Since the length of the cysteine side chain is comparable to aspartate, we conclude a bridged binding also for D212. The remaining three histidines mutated in this study (H231, H248, and H270) all show strongly reduced phosphodiesterase activity. Thus, on the basis of the kinetics investigation they are all candidates for metal binding. The EXAFS study of wild-type ZiPD showed an average coordination number of 4.5 ± 0.5 (*1*). The coordination number of zinc in proteins is generally 4 or 5 (*36*). Since our proposal involves D68, H69, D212, and the bridging water ligand, only one of these histidines can occupy the fifth binding site. The most striking difference in the kinetics of the alanine mutants is that H231A and H270A show a significantly increased K', which is indicative of reduced substrate affinity. In contrast, K' for H248A is slightly reduced. Mutation of zinc ligands in metallo-β-lactamases often resulted in an increase in K_M (*37*−*39*), which is in agreement with an involvement of the zinc atoms in substrate binding. The interesting result of this kinetic study is that alteration of residues that bind ZnA (H141), both metal ions (D212), or ZnB (H69) does not change K'. A change in the electronic properties of the zinc atom should result in a change in K' if it is responsible for substrate binding. Since the replacement of the residues analyzed here does not affect K', the mechanism for bpNPP cleavage must be different from that of the metallo-β-lactamases. Here, the binuclear zinc site does not bind the substrate directly and functions mainly in supplying the nucleophile. Given this hypothesis, the fifth coordination site of ZnB is supposed to be occupied by H248, because its replacement does not change K' significantly. A definite proof, however, can only be given when a three-dimensional structure is available. On the basis of the current experiments a zinc coordination by H231 or H270 cannot finally be

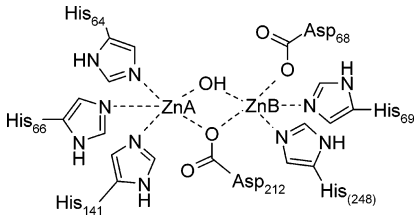

FIGURE 6: Model of the zinc coordination of ZiPD. ZiPD binuclear zinc site as derived in this study is from kinetic and EXAFS analysis of site-directed mutants. The parentheses indicate that despite the current experiments supporting His248 as the Zn ligand, we cannot absolutely exclude the possibility that this position might be held by His231 or His270.

excluded, but H248 is currently the most reasonable. This results in the final model of the binuclear zinc site of ZiPD as shown in Figure 6. This new model of the ZiPD zinc coordination is within the error range of the previous model (*1*), which was solely based on the EXAFS analysis of ZiPD wild type.

A decrease of the Hill coefficient was observed for H248A and H270A, indicative of a potential involvement in cooperativity. A detailed interpretation of this finding requires knowledge about the structural arrangement of the ZiPD homodimer.

H231 and H270 are directly or remotely responsible for binding the artificial substrate bpNPP. Since this is a rather simple substrate when compared to the possible substrate tRNA, these residues (or the regions they are placed in) should be of general importance of phosphodiester recognition by ZiPD. It is noteworthy that homologous metal coordinating residues in human ElaC 2 are found in the C-terminal part only and not in the N-terminal part. In agreement with that, a 3′ tRNA processing activity was not observed with a human ElaC 2 construct missing the C-terminal domain (*4*).

The surprising observation when comparing the ZiPD metal site model to that of other metallo-β-lactamase domain proteins is that the coordinating residues are identical to GlxII. This is substantiated by comparing the Zn EXAFS spectra for both enzymes (Figure 5). The fact that both metal sites are similar supports the view that it is not the metal coordination alone which governs the substrate specificity. Moreover, it was recently shown that GlxII is more flexible in its metal requirement than ZiPD, as GlxII is active with different ratios of zinc, manganese, and iron, whereas ZiPD is active with zinc only (*1*, *13*). Thus, also the preference for the metal used for catalysis is determined by factors outside the metal coordination sphere.

ACKNOWLEDGMENT

We thank Dr. André Matagne, University of Liège, Belgium, for help in recording the CD spectra and Brenda Kostelecky (EMBL Hamburg) for technical assistance and carefully reading the manuscript.

SUPPORTING INFORMATION AVAILABLE

One figure showing the CD spectra of the ZiPD mutants used in this study. This material is available free of charge via the Internet at http://pubs.acs.org.

REFERENCES

1. Vogel, A., Schilling, O., Niecke, M., Bettmer, J., and Meyer-Klaucke, W. (2002) ElaC encodes a novel binuclear zinc phosphodiesterase, *J. Biol. Chem. 277*, 29078−29085.
2. Tavtigian, S. V., Simard, J., Teng, D. H., Abtin, V., Baumgard, M., Beck, A., Camp, N. J., Carillo, A. R., Chen, Y., Dayananth, P., Desrochers, M., Dumont, M., Farnham, J. M., Frank, D., Frye, C., Ghaffari, S., Gupte, J. S., Hu, R., Iliev, D., Janecki, T., Kort, E. N., Laity, K. E., Leavitt, A., Leblanc, G., McArthur-Morrison, J., Pederson, A., Penn, B., Peterson, K. T., Reid, J. E., Richards, S., Schroeder, M., Smith, R., Snyder, S. C., Swedlund, B., Swensen, J., Thomas, A., Tranchant, M., Woodland, A. M., Labrie, F., Skolnick, M. H., Neuhausen, S., Rommens, J., and Cannon-Albright, L. A. (2001) A candidate prostate cancer susceptibility gene at chromosome 17p, *Nat. Genet. 27*, 172−180.
3. Schiffer, S., Rosch, S., and Marchfelder, A. (2002) Assigning a function to a conserved group of proteins: the tRNA 3′-processing enzymes, *EMBO J. 21*, 2769−2777.
4. Takaku, H., Minagawa, A., Takagi, M., and Nashimoto, M. (2003) A candidate prostate cancer susceptibility gene encodes tRNA 3′ processing endoribonuclease, *Nucleic Acids Res. 31*, 2272−2278.
5. Li, Z., and Deutscher, M. P. (2002) RNase E plays an essential role in the maturation of *Escherichia coli* tRNA precursors, *RNA 8*, 97−109.
6. Schurer, H., Schiffer, S., Marchfelder, A., and Morl, M. (2001) This is the end: processing, editing and repair at the tRNA 3′-terminus, *Biol. Chem. 382*, 1147−1156.
7. Pellegrini, O., Nezzar, J., Marchfelder, A., Putzer, H., and Condon, C. (2003) Endonucleolytic processing of CCA-less tRNA precursors by RNase Z in *Bacillus subtilis*, *EMBO J. 22*, 4534−4543.
8. Daiyasu, H., Osaka, K., Ishino, Y., and Toh, H. (2001) Expansion of the zinc metallo-hydrolase family of the beta-lactamase fold, *FEBS Lett. 503*, 1−6.
9. Aravind, L. (1999) An evolutionary classification of the metallo-beta-lactamase fold proteins, *In Silico Biol. 1*, 69−91.
10. Cameron, A. D., Ridderstrom, M., Olin, B., and Mannervik, B. (1999) Crystal structure of human glyoxalase II and its complex with a glutathione thiolester substrate analogue, *Struct. Folding Des. 7*, 1067−1078.
11. Carfi, A., Pares, S., Duee, E., Galleni, M., Duez, C., Frère, J. M., and Dideberg, O. (1995) The 3-D structure of a zinc metallo-beta-lactamase from *Bacillus cereus* reveals a new type of protein fold, *EMBO J. 14*, 4914−4921.
12. Callebaut, I., Moshous, D., Mornon, J. P., and de Villartay, J. P. (2002) Metallo-beta-lactamase fold within nucleic acids processing enzymes: the beta-CASP family, *Nucleic Acids Res. 30*, 3592−3601.
13. Schilling, O., Wenzel, N., Naylor, M., Vogel, A., Crowder, M. W., Makaroff, C. A., and Meyer-Klaucke, W. (2003) Flexible metal binding of the metallo-β-lactamase domain: glyoxalase II incorporates iron, manganese, and zinc in vivo, *Biochemistry 42*, 11777−11786.
14. Frazao, C., Silva, G., Gomes, C. M., Matias, P., Coelho, R., Sieker, L., Macedo, S., Liu, M. Y., Oliveira, S., Teixeira, M., Xavier, A. V., Rodrigues-Pousada, C., Carrondo, M. A., and Le Gall, J. (2000) Structure of a dioxygen reduction enzyme from desulfovibrio gigas, *Nat. Struct. Biol. 7*, 1041−1045.
15. Concha, N. O., Rasmussen, B. A., Bush, K., and Herzberg, O. (1996) Crystal structure of the wide-spectrum binuclear zinc beta-lactamase from Bacteroides fragilis, *Structure 4*, 823−836.
16. Ullah, J. H., Walsh, T. R., Taylor, I. A., Emery, D. C., Verma, C. S., Gamblin, S. J., and Spencer, J. (1998) The crystal structure of the L1 metallo-beta-lactamase from *Stenotrophomonas maltophilia* at 1.7 angstrom resolution, *J. Mol. Biol. 284*, 125−136.
17. Melino, S., Capo, C., Dragani, B., Aceto, A., and Petruzzelli, R. (1998) A zinc-binding motif conserved in glyoxalase II, beta-lactamase and arylsulfatases, *Trends Biochem. Sci. 23*, 381−382.
18. Thompson, J. D., Higgins, D. G., and Gibson, T. J. (1994) CLUSTAL W: improving the sensitivity of progressive multiple sequence alignment through sequence weighting, position-specific gap penalties and weight matrix choice, *Nucleic Acids Res. 22*, 4673−4680.
19. Turchin, A., and Lawler, J. F., Jr. (1999) The primer generator: a program that facilitates the selection of oligonucleotides for site-directed mutagenesis, *Biotechniques 26*, 672−676.
20. Segel, I. H. (1993) *Enzyme Kinetics*, Wiley Classics Library Edition, John Wiley & Sons, New York.
21. Pettifer, R. F., and Hermes, C. (1985) Absolute energy calibration of X-ray radiation from synchrotron sources, *J. Appl. Crystallogr. 18*, 404−412.
22. Binsted, N., Strange, R. W., and Hasnain, S. S. (1992) Constrained and restrained refinement in EXAFS data analysis with curved wave theory, *Biochemistry 31*, 12117−12125.

23. Feiters, M. C., Eijkelenboom, A. P., Nolting, H. F., Krebs, B., Van Den Ent, F. M., Plasterk, R. H., Kaptein, R., and Boelens, R. (2003) X-ray absorption spectroscopic studies of zinc in the N-terminal domain of HIV-2 integrase and model compounds, *J. Synchrotron Radiat. 10*, 86−95.
24. de Seny, D., Heinz, U., Wommer, S., Kiefer, M., Meyer-Klaucke, W., Galleni, M., Frère, J. M., Bauer, R., and Adolph, H. W. (2001) Metal ion binding and coordination geometry for wild type and mutants of metallo-beta-lactamase from *Bacillus cereus* 569/H/9 (BcII): a combined thermodynamic, kinetic, and spectroscopic approach, *J. Biol. Chem. 276*, 45065−45078.
25. Harding, M. M. (1999) The geometry of metal−ligand interactions relevant to proteins, *Acta Crystallogr. D 55*, 1432−1443.
26. Harding, M. M. (2001) Geometry of metal−ligand interactions in proteins, *Acta Crystallogr. D 57*, 401−411.
27. Mijovilovich, A., and Meyer-Klaucke, W. (2001) Determination of metal−metal distances: significance and accuracy, *J. Synchrotron Radiat. 8*, 692−694.
28. Riggs-Gelasco, P. J., Stemmler, T. L., and Penner-Hahn, J. E. (1995) XAFS of dinuclear metal sites in proteins and model compounds, *Coord. Chem. Rev. 144*, 245−286.
29. Lin, Y., Dotsch, V., Wintner, T., Peariso, K., Myers, L. C., Penner-Hahn, J. E., Verdine, G. L., and Wagner, G. (2001) Structural basis for the functional switch of the *E. coli* Ada protein, *Biochemistry 40*, 4261−4271.
30. Jacquamet, L., Aberdam, D., Adrait, A., Hazemann, J. L., Latour, J. M., and Michaud-Soret, I. (1998) X-ray absorption spectroscopy of a new zinc site in the fur protein from *Escherichia coli*, *Biochemistry 37*, 2564−2571.
31. Peariso, K., Zhou, Z. S., Smith, A. E., Matthews, R. G., and Penner-Hahn, J. E. (2001) Characterization of the zinc sites in cobalamin-independent and cobalamin-dependent methionine synthase using zinc and selenium X-ray absorption spectroscopy, *Biochemistry 40*, 987−993.
32. Tobin, D. A., Pickett, J. S., Hartman, H. L., Fierke, C. A., and Penner-Hahn, J. E. (2003) Structural characterization of the zinc site in protein farnesyltransferase, *J. Am. Chem. Soc. 125*, 9962−9969.
33. Mijovilovich, A., and Meyer-Klaucke, W. (2003) Simulating the XANES of metalloenzymes−a case study, *J. Synchrotron Radiat. 10*, 64−68.
34. Wang, Z., Fast, W., Valentine, A. M., and Benkovic, S. J. (1999) Metallo-beta-lactamase: structure and mechanism, *Curr. Opin. Chem. Biol. 3*, 614−622.
35. Wang, Z., Fast, W., and Benkovic, S. J. (1999) On the mechanism of the metallo-beta-lactamase from *Bacteroides fragilis*, *Biochemistry 38*, 10013−10023.
36. Auld, D. S. (2001) Zinc coordination sphere in biochemical zinc sites, *BioMetals 14*, 271−313.
37. Yanchak, M. P., Taylor, R. A., and Crowder, M. W. (2000) Mutational analysis of metallo-beta-lactamase CcrA from *Bacteroides fragilis*, *Biochemistry 39*, 11330−11339.
38. Crowder, M. W., Wang, Z., Franklin, S. L., Zovinka, E. P., and Benkovic, S. J. (1996) Characterization of the metal-binding sites of the beta-lactamase from *Bacteroides fragilis*, *Biochemistry 35*, 12126−12132.
39. de Seny, D., Prosperi-Meys, C., Bebrone, C., Rossolini, G. M., Page, M. I., Noel, P., Frère, J. M., and Galleni, M. (2002) Mutational analysis of the two zinc-binding sites of the *Bacillus cereus* 569/H/9 metallo-beta-lactamase, *Biochem. J. 363*, 687−696.
40. Eggers-Borkenstein, P., Priggemeyer, S., Krebs, B., Henkel, G., Simonis, U., Pettifer, R. F., Nolting, H. F., and Hermes, C. (1989) Extended X-ray absorption fine structure (EXAFS) investigations of model compounds for zinc enzymes, *Eur. J. Biochem. 186*, 667−675.

BI049703+